TEST AND EVALUATION OF AN INLET BARRIER FILTER TO INCREASE ENGINE TIME-ON-WING FOR THE BELL BOEING V-22 OSPREY TILTROTOR

by

VICTOR HWA

Presented to the Faculty of the Graduate School of

The University of Texas at Arlington in Partial Fulfillment

of the Requirements

for the Degree of

MASTER OF SCIENCE IN AEROSPACE ENGINEERING

THE UNIVERSITY OF TEXAS AT ARLINGTON

MAY 2015

Acknowledgements

First of all, I would like to thank Dr. Don Wilson for agreeing to chair my thesis committee, and to Dr. Frank Lu, Dr. Bob Mullins, and Dr. Albert Brand for agreeing to serve on my committee. I would also like to thank all of those at Bell Helicopter who reviewed this thesis and provided inputs so that my work could be approved, and would like to extend a special thanks to Dave Loe and Ted Trept for their inputs to improve the quality of my work. I would also like to especially acknowledge Dan Simpson for his assistance with the Power Assurance Check data reduction and creating many of the graphics and models used to better illustrate the prototype Engine Inlet Barrier Filter (EIBF) installation.

The concept of an EIBF for the V-22 was conceived several years before I joined Bell Helicopter. The final detail layouts were being completed when I joined the company in 2010, and I joined the team in 2012 as the Computational Fluid Dynamics (CFD) validation was successfully finalized and we started to transition to flight test. I want to acknowledge and thank the engineers who completed this work on the prototype EIBF before I joined the program.

While my main contribution to the prototype EIBF test program was reducing and analyzing the inlet distortion and pressure recovery data during the flight test, the overall success of this test program would not have been possible without a team effort from everyone else involved. I would like to acknowledge all of our Bell test pilots, flight test engineering team, instrumentation, and aircraft maintainers for doing their part to ensure that every flight was a success, as well as the engineering management and staff at Bell, Donaldson, and Rolls-Royce that worked tirelessly to ensure the success of the test program. I am deeply grateful to Bell Helicopter for being supportive of my educational pursuits and for sponsoring my graduate work and research.

Lastly, I would also like to thank all of my friends and family for their support throughout my years while I was enrolled in graduate school. I would especially like to thank my sister Stephanie, and my parents Zhih-Li and Joyce. There are not enough words that can describe how much my parents have sacrificed so that their children could receive an education, and for instilling the principles of hard-work and dedication in their children.

April 27, 2015

Abstract

TEST AND EVALUATION OF AN INLET BARRIER FILTER TO INCREASE ENGINE TIME-ON-WING FOR THE BELL BOEING V-22 OSPREY TILTROTOR

Victor Hwa, MS

The University of Texas at Arlington, 2015

Supervising Professor: Don Wilson

The Bell Boeing V-22 Osprey Tiltrotor has seen significant deployment to austere environments where airborne sand and dust is generated due to aircraft operation on, or near, the ground. Current V-22 production aircraft are equipped with an engine air particle separator (EAPS) to remove larger particles of sand and dust, but finer particulates remain an issue for engine combustion air. A prototype engine inlet barrier filter (EIBF) has been developed as a more robust particle filtration solution. Inlet air filtration with the prototype EIBF is expected to quadruple engine time-on-wing by preventing nearly all fine particulates from entering the engine. The prototype EIBF was installed on the left side of an MV-22 aircraft and was flight tested at the Bell Xworx facility in Arlington, TX with an inlet rake installed at the compressor face of the left-hand-side engine (#1 engine) to measure inlet pressures and temperatures. The author used this data to quantify inlet pressure recovery and inlet flow distortion. Measured data were correlated with analytical results obtained from Computational Fluid Dynamics (CFD); however, this thesis will focus on the flight test aspect of the test and omit technical details regarding the comparison between flight test and CFD. The inlet distortion analysis showed that stable engine operation was achieved with the inlet barrier filter

installed. Engine performance was quantified by using Power Assurance Check data generated by the V-22 Vibration, Structural Life, and Engine Diagnostic System (VSLED) on-board the aircraft, where the treated engine (inlet barrier filter installed) was compared to the baseline production inlet configuration. Austere (sand environment) flight tests were conducted at Albuquerque, NM and salt water environment tests were conducted at Pensacola, FL. The inlet barrier filter treatment resulted in a system that maintained engine performance significantly longer than the baseline air particle separator.

Table of Contents

List of Illustrations

List of Tables

List of Acronyms and Nomenclature

ADAS	Airborne Data Acquisition System
ATTR	Advanced Technology Tiltrotor
CAFTA	Computer-Aided Flight Test Analysis
CDI	Circumferential Distortion Index
CFD	Computational Fluid Dynamics
EAPS	Engine Air-Particle Separator
EDAU	Enhanced Data Acquisition Unit
EIBF	Engine Inlet Barrier Filter
FOD	Foreign Object Damage
Hp	Pressure Altitude
KAFB	Kirtland Air Force Base
KCAS	Knots Calibrated Airspeed
KTAS	Knots True Airspeed
MEDAU	Miniature Enhanced Data Acquisition Unit
MGT	Measured Gas Temperature
Ng	Engine Gas Generator Speed
Ng_c	Corrected Engine Gas Generator Speed
Np	Engine Output Shaft Speed
OAT	Outside Air Temperature
PAC	Power Assurance Check
PAV	Ring Average Total Pressure
PAVLOW	Average total-pressure of low total-pressure region for a ring
PFAV	Face Average Total Pressure
Q	Number of low-pressure regions

Qe	Engine Torque
RDI	Radial Distortion Index
TOW	Time-On-Wing
USAF	United States Air Force
USMC	United States Marine Corps
V/STOL	Vertical and Short Take Off Landing
VSLED	Vibration Structural Life and Engine Diagnostics
θ^-	Extent of low-pressure region

Chapter 1

INTRODUCTION

1.1 Bell Boeing V-22 Tiltrotor Aircraft Background

The Bell Boeing V-22 Osprey (V-22) is a multi-mission vertical and short take off landing (V/STOL) air vehicle. As the world's first production tiltrotor aircraft in service with the United States Marine Corps (USMC) and the United States Air Force (USAF), it has the speed, range, altitude, and endurance of fixed wing transports combined with the ability to take off and land similar to conventional helicopters. This is accomplished by rotating the nacelles from 0° (airplane mode) to 90° (helicopter mode), which gives the aircraft a unique blend of speed, range, altitude, and survivability for maximum effectiveness in completing its missions. The V-22 can achieve altitudes up to 25,000 feet and cruise at speeds in excess of 250 knots true airspeed (KTAS) in airplane mode [1]. The aircraft has accumulated more than 250,000 flight hours, including multiple combat tours in austere environments laden with sand, salt, and other fine particulate matter. The United States Marine Corps operates the MV-22 variant, while the United States Air Force operates the CV-22 variant; when the term V-22 is used in this thesis, it refers to both variants. A photograph of the V-22 Osprey in service with the United States Marine Corps is shown in Figure 1.1 [2].

Figure 1.1 MV-22 landing on the USS Kearsarge

The V-22 is powered by two Rolls-Royce AE 1107C turboshaft gas-turbine engines. The AE 1107C engine, shown in Figure 1.2 [3], has a two-shaft axial compressor consisting of a 14-stage compressor followed by an effusion-cooled annular combustor, a two-stage high pressure turbine, and a two-stage low pressure turbine [3]. Since the V-22 has seen significant deployment to saltwater and austere environments where airborne sand and dust is generated due to aircraft operation on, or near, the ground, particle filtration is essential to protect the engine from erosion and prolong the life of the engine. Figure 1.3 depicts a CV-22 operating over an austere environment in airplane mode [4].

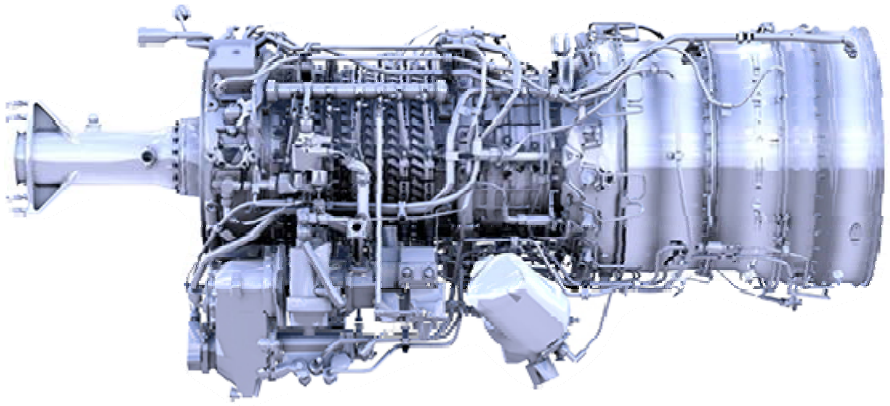

Figure 1.2 Rolls-Royce AE 1107C Engine

Figure 1.3 CV-22 Operating in Airplane Mode over Austere Environment

1.2 Engine Particle Filtration Challenges

Current production V-22 aircraft feature an engine inlet incorporating an integral, self-cleaning inertial engine air-particle separator (EAPS). Particulate air enters the inlet and makes a sharp turn; the inertia of the particles make them tend to go into a scavenge duct while the clean air enters the compressor. Blowers located in the forward-lower portion of each nacelle pull the scavenge flow through exit ducts which dump the particles and scavenge air overboard.

Although the current production EAPS is effective at removing coarse particles, finer particulates remain an issue for engine air. Due to different soil composition and prevalent sand and dust storms in some operational environments, fine particulate matter can pass the current-production EAPS without being captured in the scavenge ducts. This causes rapid degradation of the compressor blades, leading to more frequent maintenance intervals and reduced engine time-on-wing. Consequently, aircraft down time is increased, resulting in higher operating and maintenance costs for the V-22 customer.

1.3 Prototype Engine Inlet Barrier Filter (EIBF)

To better address the issue of engine particle filtration challenges, a prototype engine inlet barrier filter (EIBF) has been developed as a more robust particle filtration solution (Figure 1.4). Inlet air filtration with the prototype EIBF is expected to substantially increase engine time-on-wing (TOW) by preventing nearly all fine particulates from entering the engine. The prototype V-22 EIBF system was designed by Bell Helicopter engineers and manufactured by Donaldson Filtration Solutions. It consists of a modified inlet cowling with a hinged door (bypass door) and four oil-wetted filter assemblies spanning around the bottom edge of the nacelle, as seen in Figure 1.5. Figure 1.6 depicts the structure of the prototype EIBF prior to installation on the flight test aircraft. The

bypass door operation is governed by an electromechanical actuator and differential pressure sensor and switch. During hover and when the aircraft is operating in austere environments, the bypass door is closed to ensure the intake air is filtered. If the inlet plenum pressure is detected to reach an elevated level due to blockage on the filters, the differential pressure sensor commands the switch to open the bypass door and allows the airflow to bypass the filters. The bypass door is opened during airplane-mode flight at higher altitudes to increase inlet recovery and reduce drag, in order to maximize cruise performance.

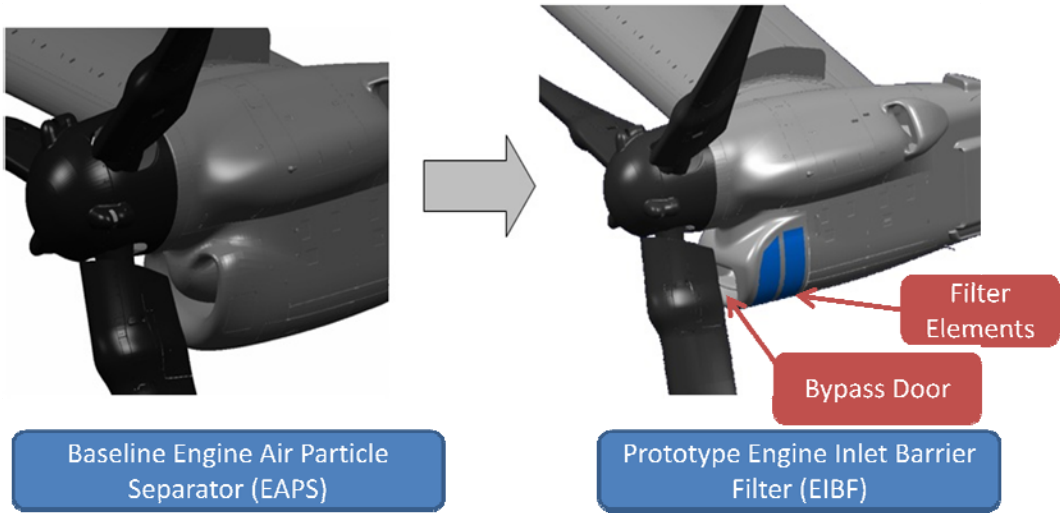

Figure 1.4 Modification from Production Inlet Configuration with EAPS to Prototype EIBF System

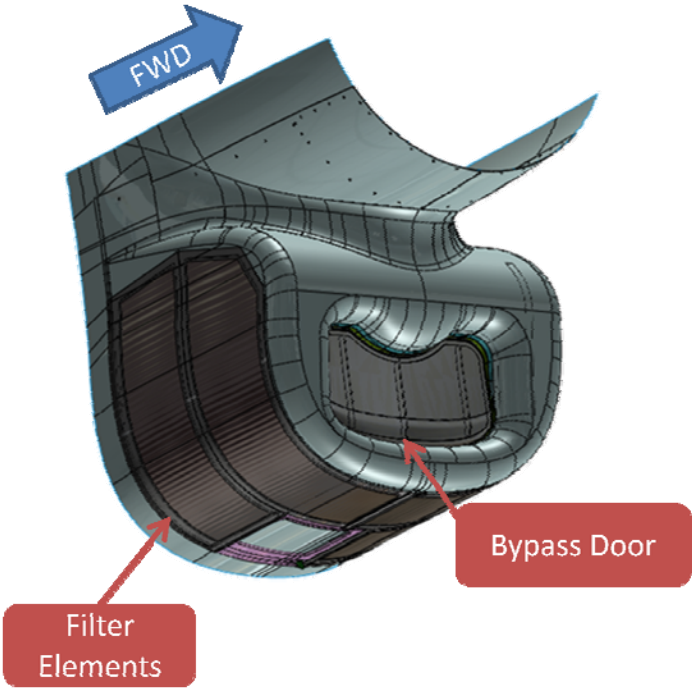

Figure 1.5 Prototype EIBF System

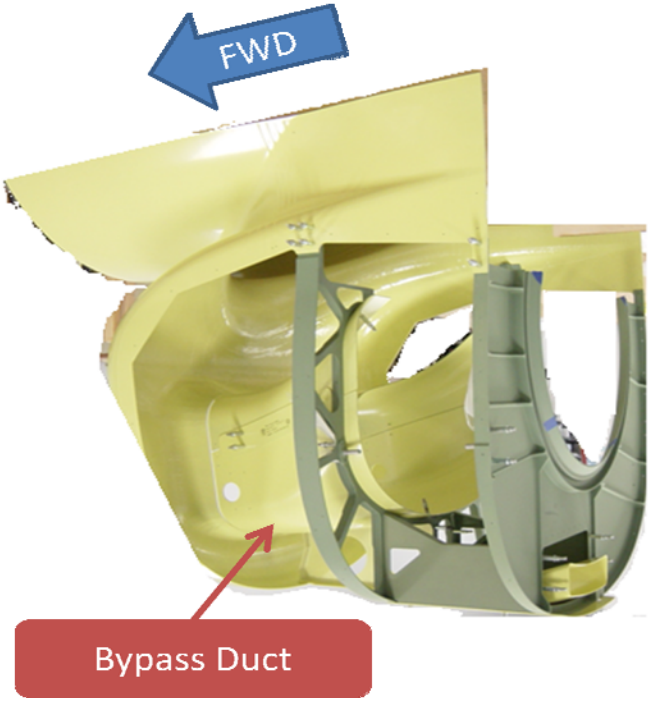

Figure 1.6 Structure of Prototype EIBF

1.3.1 Inlet Design Principles

Since the inlet directly interfaces with the internal airflow and the flow around the aircraft, it has a major impact on engine and aircraft performance [5]. Therefore, inlets are designed to maximize pressure recovery as well as for a uniform flow with minimal pressure and temperature distortion at the compressor front face. For the prototype EIBF design, the author is interested in applying these principles by ensuring that the design has a high inlet pressure recovery as well as high pressure distortion margin when compared to the distortion limit of the AE 1107C engine during flight test. Inlet pressure distortion is defined as spatial variations in the total pressure at the inlet/engine interface plane; a complete description of inlet distortion can be found in SAE ARP1420 [6].

1.3.2 Analytical Validation of Prototype EIBF

Prior to commencing flight testing of the prototype EIBF system, Computational Fluid Dynamics (CFD) simulations of the prototype EIBF installation were run using the FLEUNT™ CFD software package to evaluate inlet pressure distortion and recovery at various altitudes and airspeeds with the bypass door either closed or open in all flight modes: helicopter mode (90° nacelle), conversion (between 0° - 90° nacelle), and airplane mode (0° nacelle). The CFD simulations showed that the prototype EIBF installation would have sufficient inlet pressure distortion margin and demonstrated the feasibility of the prototype EIBF design, leading to its implementation on a V-22 aircraft for flight test demonstration and evaluation.

Chapter 2

FLIGHT TEST BACKGROUND

2.1 Overview and Objectives

The purpose of the prototype EIBF flight testing was to determine the feasibility and evaluate the technical characteristics of the installation. Based on the inlet design principles described in Section 1.3.1, the following objectives were developed and evaluated through the course of the flight tests:

1. Ensure safety of flight with the prototype EIBF installation, including aircraft, engine, and EIBF bypass door operation
2. Ensure adequate inlet and engine performance of the engine with the prototype EIBF installation, including pressure recovery, inlet pressure distortion, and engine power levels when compared to the engine without the prototype EIBF installed.
3. Compare degradation of the engine with the prototype EIBF installed to the engine without the prototype EIBF installed.

Flight testing was conducted from June 2012 through December 2013, with an overview of the testing provided in Table 2.1.

Table 2.1 Overview of Flight Test

Phase	Location	Description
I	Arlington, TX	EIBF Design Evaluation and Envelope Expansion. Clean air, non-austere environment testing to ensure adequate inlet distortion margin, pressure recovery and engine power levels.
II	Albuquerque, NM	Austere environment testing to ensure adequate engine power levels, compare performance of prototype EIBF engine to production inlet and filter maintenance intervals (time between cleanings). No pressure recovery or distortion data collected.
III	Arlington, TX	Continued design development and envelope expansion. Clean air, non-austere environment testing to improve inlet distortion margin during airplane door cruise with bypass door open.
IV	Pensacola, FL	Saltwater environment testing to ensure adequate engine power levels and to compare performance of prototype EIBF engine to production inlet. No pressure recovery or distortion data collected.

2.2 Aircraft Background and Configuration

Flight testing was accomplished on an MV-22 aircraft that was leased by the Bell Boeing team from the United States Department of Defense; this aircraft was dubbed the Advanced Technology Tiltrotor (ATTR). The EAPS was removed from the left side nacelle of the ATTR and the prototype EIBF was installed in its place (#1 engine). Figure 2.1 depicts the prototype EIBF as installed in front of the #1 engine on the test aircraft from an outboard-looking-inboard view, while Figure 2.2 shows the inlet plenum in a forward-looking-aft view. The red cover that can be seen in Figure 2.2 is the location of the engine interface plane where the inlet rake is installed for Phase I and III testing, and is described in more detail in Section 2.3.1. The right hand side nacelle retained the current production inlet with the EAPS, and remained unchanged (#2 engine). With

exception of the data acquisition and instrumentation package, all other aspects of the aircraft are representative of the current production aircraft and remain unchanged, including the Rolls-Royce AE1107C engines and the on-board V-22 Vibration, Structural Life, and Engine Diagnostic System (VSLED) [7]. The VSLED Power Assurance Check function was used to assess engine health during these flight tests using proprietary algorithms.

For each flight test conducted, the ATTR aircraft was loaded to mid gross weight and mid aircraft center of gravity for all flight tests. The aircraft was operated by Bell Helicopter test pilots, with engineering support provided by Bell Helicopter flight test and propulsion engineers including the author. Since there was no real-time telemetry, critical parameters were monitored on board by flight test engineers and collected data were reduced and analyzed post-flight by the author.

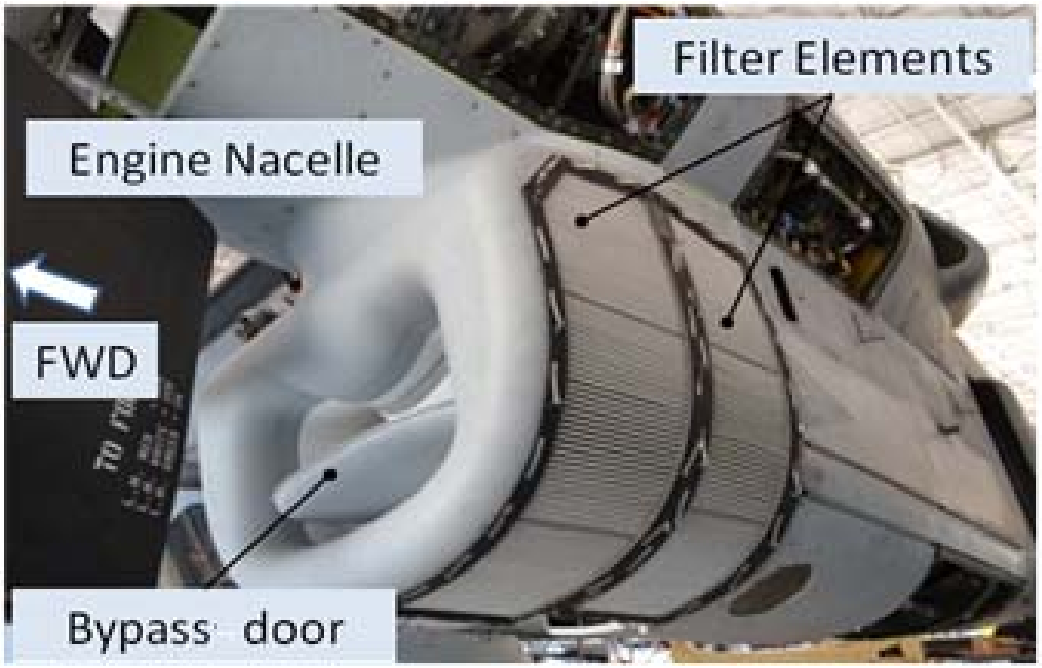

Figure 2.1 EIBF Installation (outboard-looking-inboard view)

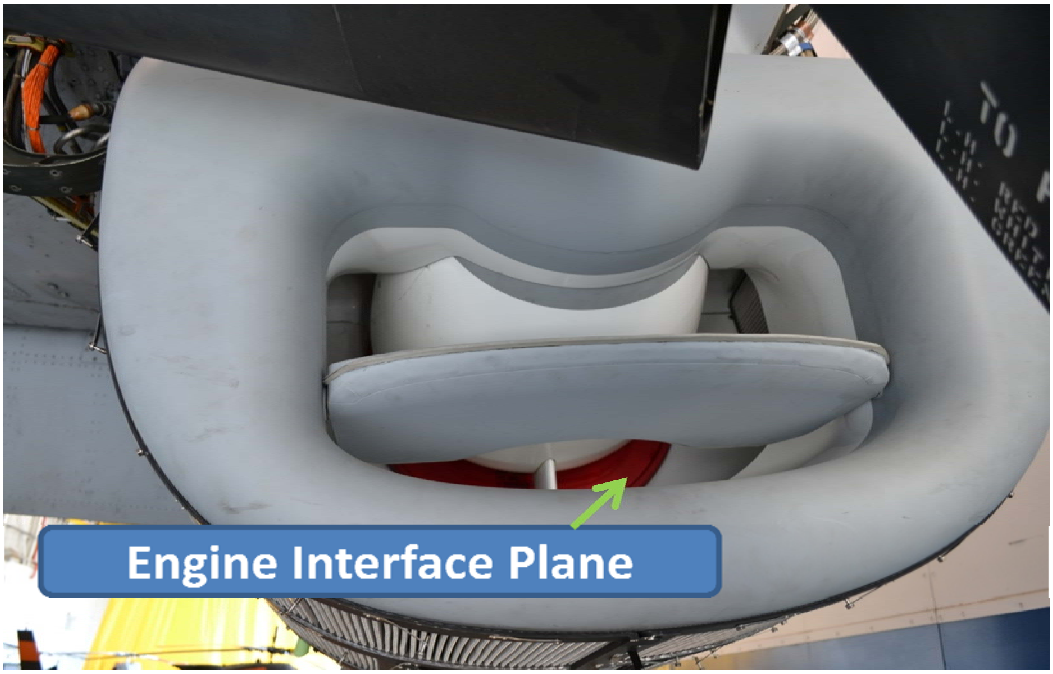

Figure 2.2 Inlet plenum (forward-looking-aft view)

2.3 Instrumentation

Based on the inlet design principles listed in section 1.3.1, the instrumention listed in Table 2.2 was recommended and installed on ATTR for the flight tests. A schematic of the inlet rake along with a table of the pressure and temperature probes on the rake is located in Appendix A. All inlet rake pressure measurements were referenced to a static pressure sensor located in the #1 engine nacelle.

Table 2.2 ATTR Instrumentation Listing

No.	Parameter	Description	Units
1.	OAT	Ambient Temperature	°C
2.	Hp	Pressure Altitude	Feet
3.	KCAS	Airspeed	KCAS
4.	#1 engine Ng #2 engine Ng	Engine Gas Generator Speed	% rpm
5.	#1 engine Np #2 engine Np	Engine Output Shaft Speed	% rpm
6.	#1 engine Qe #2 engine Qe	Engine Torque	ft. lb.
7.	#1 engine MGT #2 engine MGT	Engine Measured Gas Temperature	°C
8.	dP Pressure dP Pressure (backup)	Inlet Plenum Pressure	Psid
9.	Reference Pressure	Static pressure measurement collected in #1 nacelle to reference differential pressures No. 8, 10 & 11	psia
10.	See Section 2.3.1 & Table A.1 in Appendix A	Inlet rake total pressure probes, 1 through 40	psid
11.	See Section 2.3.1 & Table A.2 in Appendix A	Inlet rake static pressure probes, 1 through 8	psid
12.	See Section 2.3.1 & Table A.3 in Appendix A	Inlet rake total temperature probes, 1 through 24	°C

2.3.1 Steady State Inlet Rake Assembly (Phase I & III Only)

A steady-state inlet rake assembly was installed on the inlet bellmouth of the #1 engine during Phase I and III flight testing. The inlet rake assembly consisted of eight rakes equally spaced at 45° intervals around the bellmouth as seen in Figure 2.3, which was built in accordance with the guidelines outlined in SAE ARP 1420B [6]. Each rake consisted of five total pressure probes and three total temperature probes. Together, there were 40 total pressure probes and 24 total temperature probes; the total pressure probes and total temperature probes were centered in equal annular areas. There were also eight static pressure sensors equally spaced in between each rake on the wall of the inlet bellmouth. Figure 2.4 shows the installation of the inlet rake on the engine interface plane, which is near the face of the engine compressor.

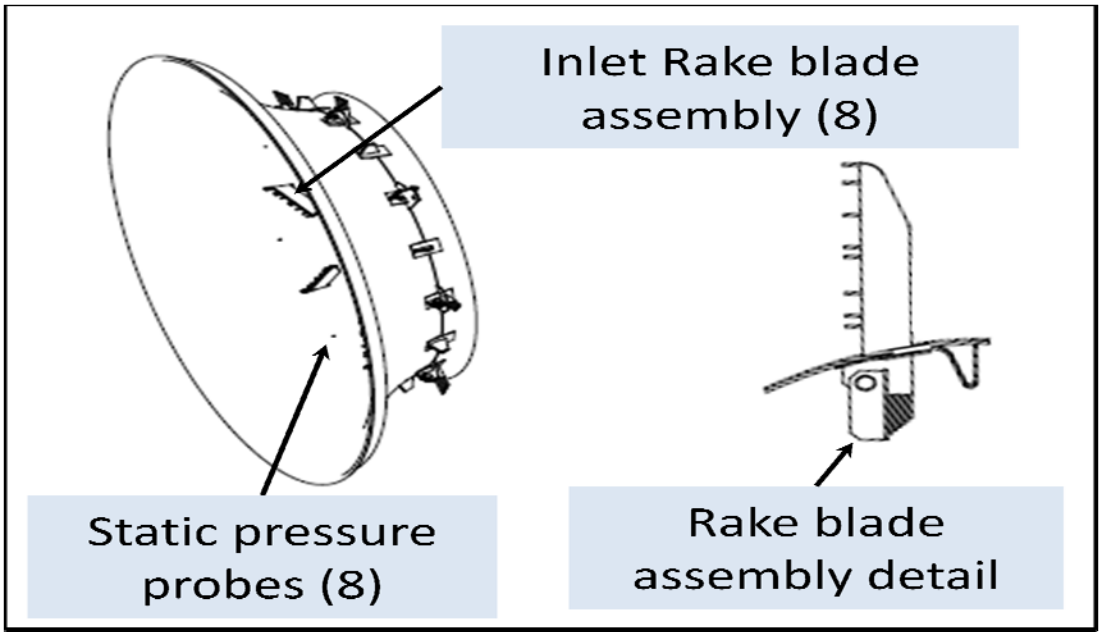

Figure 2.3 Inlet Rake Assembly

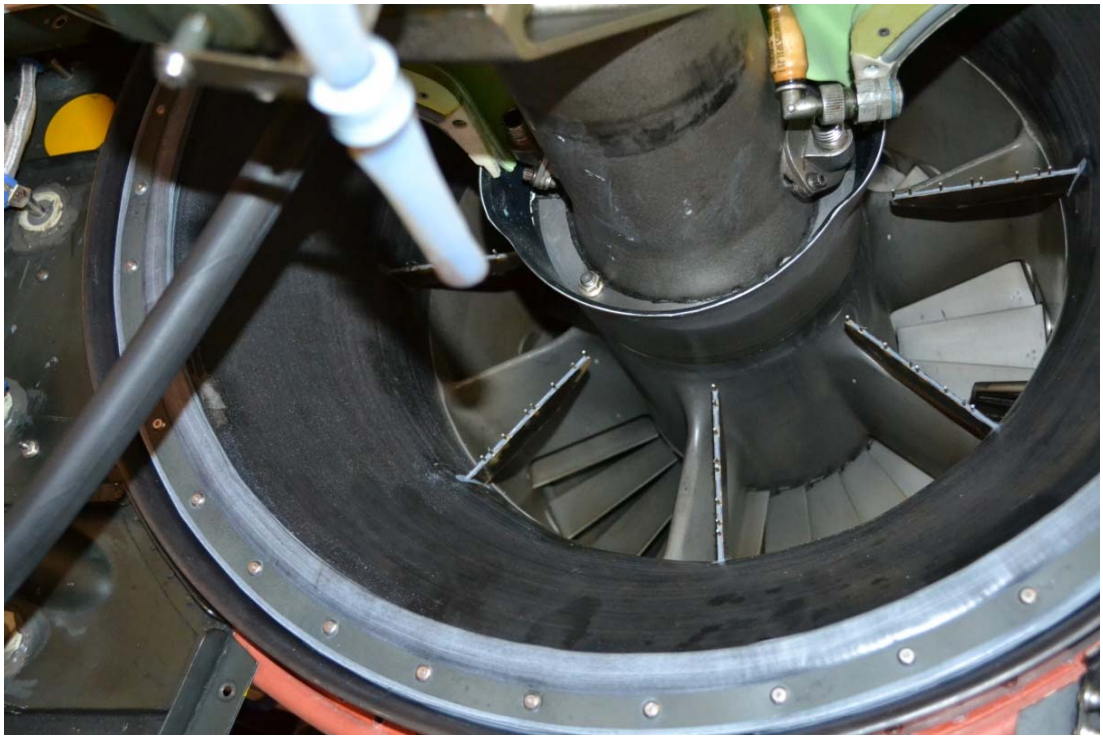

Figure 2.4 Inlet Rake Installation and Engine Interface Plane

2.3.2 Data Acquisition

The aircraft was equipped with an airborne data acquisition system (ADAS) that accurately recorded measurements from the instrumentation installed on the aircraft. The ADAS consisted of several components: an Enhanced Data Acquisition Unit (EDAU), a Miniature Enhanced Data Acquisition Unit (MEDAU) installed remotely in the engine nacelle, and the data recorder. Data collected from all instrumentation sources were encoded into a unified digital data stream that was saved in the recorder on board the aircraft. A prime data switch was installed in the cockpit that the pilot engages prior to starting a maneuver and disengages at the end of the maneuver; the time-averaged data through the record with the prime data switch engaged are known to be a “prime record.” The data recorded from each flight were downloaded and imported into conventional spreadsheet programs after each flight test for analysis by the author.

Chapter 3

TEST PROCEDURES, RESULTS, AND DISCUSSION

3.1 Phase I

3.1.1 Purpose of Test and Test Conditions

The primary purpose of Phase I Flight testing was to expand the flight envelope by completing a matrix of test conditions to ensure stability of the #1 engine. The inlet rake assembly was installed on the #1 engine bellmouth so that pressure and temperature characteristics of the prototype EIBF installation could be assessed by the author, with the objective to verify engine stability throughout the flight envelope so that the inlet rake could be removed for austere and salt-water environment testing in Phases II and IV respectively. Progression through the flight test matrix was conducted in a conservative buildup fashion, starting with steady state ground runs. The testing then progressed into steady state flight test conditions at various altitudes and airspeeds with the bypass door either closed or open in all aircraft flight modes. During Phase I testing, one test flight was performed using simulated degraded filters, where the purpose was to collect inlet data with a set of filters that simulate a clogged filter in an austere environment. Transient maneuvers, such as throttle pulses where the pilot pulled the thrust control levers back and forth and an in-flight shutdown and restart of the #1 engine, was conducted to ensure engine stability during transient maneuvers for safety of flight purposes only. Inlet pressure distortion and recovery data were only computed by the author during steady state maneuvers such as steady climbs, level flight, and steady dives, and were not measured during transient maneuvers such as throttle pulses.

3.1.2 Flight Test Outcomes

Stable engine operation was maintained on the #1 engine; there were no instances of abnormal engine operation as a result of the prototype EIBF at any time during Phase I testing. Acquired data are presented in Sections 3.1.3 through 3.1.5. Based on the early findings of the test, design modifications were made to the prototype EIBF including blanking plates and inlet duct extensions, which are discussed in Sections 3.1.2.1 and 3.1.2.2 respectively. The blanking plate and inlet duct modifications were left installed for the entire duration of flight testing; the results presented in Sections 3.1.3 through 3.1.5 and Sections 3.2 through 3.4 present the data collected with the blanking plate and inlet duct extension modifications.

3.1.2.1 Installation of Blanking Plates

During the second flight test, several #1 engine components were recording temperatures that were slightly above what was expected during cruise flight condition with the bypass door open. The prototype EIBF bypass was sized based on the hover flight condition, which is the peak airflow condition. Since the engine requires less airflow in cruise than hover, the inlet is oversized for the cruise flight condition. Thus, some of the airflow spills out of the porous media during cruise with the bypass door open. This phenomenon interrupts the airflow path through a cooling scoop downstream of the filters; the purpose of the cooling scoop is to direct airflow to provide cooling air to critical nacelle components. Additional CFD simulations demonstrated that restricting airflow through the top portion of the filters would cause the affected engine component temperatures to fall to acceptable levels by reducing filter outflow in the affected area. Thus, to rectify this issue, blanking plates restricting flow at the top of filters were installed immediately following the flight where the issue was discovered (Figure 3.1). These blanking plates were installed in a fixed location on the upper portion of the filters on the

inboard side of the filters. Subsequent flight tests after the blanking plate installation verified that the affected component temperatures returned to acceptable temperature levels. As discussed in Section 3.1.2, the blanking plates were left installed for the duration of flight testing to ensure adequate nacelle cooling, with this lesson learned noted for a final production design configuration.

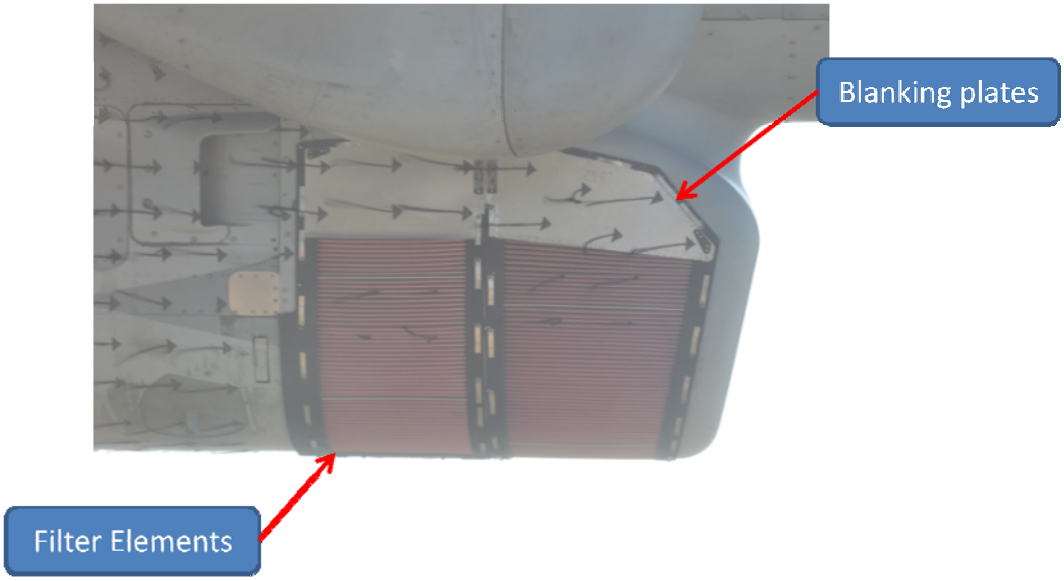

Figure 3.1 Blanking Plate Installation

3.1.2.2 Bypass Duct Modifications

During the first several Phase I flights, elevated levels of inlet pressure distortion was discovered by the author during airplane mode cruise with the bypass door open. The root cause of this issue was attributed to a low pressure region that formed in the inlet plenum. To alleviate this issue, the original inlet duct was modified and tested by adding inlet duct extensions. The purpose was to direct additional airflow to the low pressure region that was causing the elevated inlet pressure distortion levels with the bypass door open.

3.1.3 Inlet Distortion

3.1.3.1 Data Reduction

Inlet pressure and temperature distortion was calculated by the author using the measurements captured by the 40 inlet pressure probes and 24 inlet temperature probes during prime records of steady state maneuvers. Pressure and temperature data collected were reduced per Appendix A of SAE ARP1420 Revision B [6], which is considered to be a widely accepted standard of quantifying inlet distortion in the aerospace industry. The proprietary Bell Helicopter CAFTA (Computer-Aided Flight Test Analysis) software was used by the author to perform these calculations.

The two forms of pressure distortion defined by ARP1420 are circumferential and radial distortion. The author is interested in quantifying the intensity, or magnitude, of the circumferential and radial distortion elements – this is what we define as the circumferential distortion index (CDI) and radial distortion index (RDI) respectively. The greater of RDI or CDI was taken as the maximum pressure (or temperature) distortion index. While the methodology outlined in Appendix A of ARP1420 Rev B gives a detailed explanation of the inlet distortion data reduction, the paragraphs below provide the reader a brief overview.

CDI is calculated on a ring-by-ring basis and can be classified into two types of patterns: one-per-rev patterns and multiple-per-rev patterns. For each prime record, CDI is calculated for each of the 5 rings (with subscript *i* = 1 through 5), with the maximum CDI being used to represent the CDI for the prime record. CDI for both a one-per-rev and multiple-per-rev pattern is calculated as seen in equation 3.1:

$$CDI = \left(\frac{PAV - PAVLOW}{PAV}\right)_i \tag{3.1}$$

Figure 3.2 shows a 2-D representation of a one-per-rev pattern as a plot of total pressure vs. circumferential location, with a total of eight circumferential locations spaced 45° apart represented by the hollow circles [6]. PAVi is defined as the average of the eight total pressure measurements in ring *i*. θ_i^- defines the low pressure region extent, which describes the span between circumferential locations between θ_{1_i} and θ_{2_i} where the total pressure is less than PAVi. θ_{1_i} and θ_{2_i} can be found by interpolating between the hollow circles where the solid line intersects with the dashed PAVi line. PAVLOWi is defined as the average total pressure of the low pressure region; this can be found by integrating over the area of the low pressure region and dividing by θ_i^-, as seen in equation 3.2:

$$PAVLOW_i = \frac{1}{\theta_i^-}\int_{\theta_{1_i}}^{\theta_{2_i}} P(\theta)_i d\theta \tag{3.2}$$

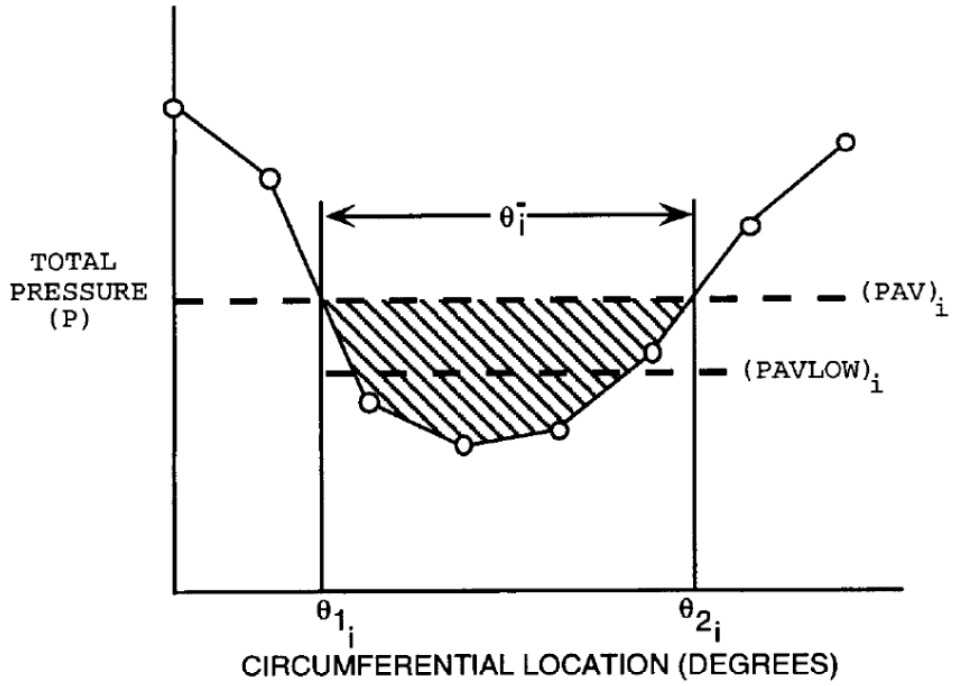

Figure 3.2 One-per-rev CDI pattern

Figure 3.3 shows a multiple-per-rev CDI pattern – notice that there is more than one low pressure region [6]. CDI for a multiple-per-rev pattern is calculated in the same manner as a one-per-rev pattern using equation 3.1.

PAVi is defined as the average of the eight total pressure measurements in ring *i*, in the same manner as a one-per-rev pattern. As seen in equation 3.3, the low pressure region extent θ_i^- is found by summation of the degrees of circumferential location.

$$\theta_i^- = \sum_{k=1}^{Q} \theta_{ik}^- \tag{3.3}$$

Q is defined as the number of low pressure regions (for example, there are two shaded regions in Figure 3.3, so Q in this case would be equal to two). Using this summation to find θ_i^- for a multiple-per-rev pattern, PAVLOWi for a multiple-per-rev pattern can be found by summation of the areas of the low pressure regions (which can be found by numerical integration) and then divided by the summation of the low pressure region extent summation, as seen in equation 3.4:

$$PAVLOW_i = \frac{1}{\theta_i^-} \sum_{k=1}^{Q} \int_{\theta_{ik}^-} P(\theta)_i d\theta \tag{3.4}$$

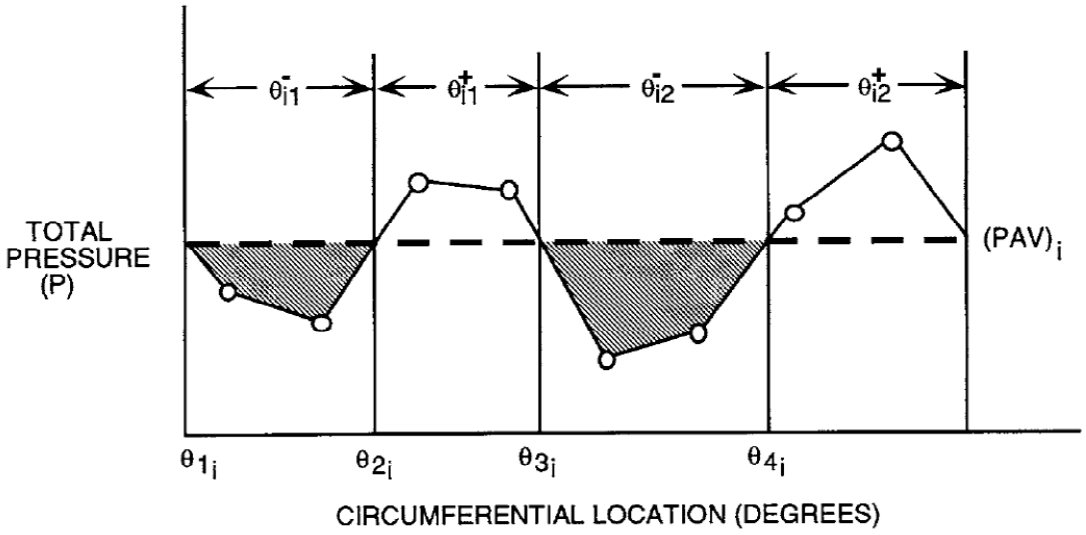

Figure 3.3 Multiple-per-rev CDI pattern

RDI is defined as the difference between the face-average pressure of the 40 pressure probes (PFAV) and the ring-average pressure of the eight pressure probes (PAV_i) in the ring *i* (where *i* again is defined as being between 1 and 5), divided by the face-average pressure (Equation 3.5).

$$RDI = \frac{PFAV - PAV_i}{PFAV} \tag{3.5}$$

Through the course of the testing, several temperature probes became inoperable. Bad temperature probes were replaced with a simple average of the values of the two adjacent temperature probes in the same ring. The simple average is an effective substitute for inoperable thermocouples because the probes are spaced in equal annular areas in the engine interface plane, and was used on previous V-22 inlet distortion tests. All pressure probes functioned normally through the course of the testing. Scatter in the inlet pressure and temperature measurements can be attributed to different engine power levels required for each test point, as well as differences in pressure altitude (Hp) and outside air temperature (OAT). Environmental variables such as Hp and OAT obviously

varied from each flight test day, which led to some inherent scatter in the test data. Scatter is not just limited to tiltrotor aircraft testing - it is not uncommon to see scatter in flight test data when performing flight testing on aircraft in general.

3.1.3.2 Results and Discussion

Inlet distortion for the prototype EIBF installation was plotted by the author as a function of pressure distortion against temperature distortion for ground runs (Figure 3.4); hover, helicopter, and conversion mode flight (Figure 3.5); as well as airplane mode (Figure 3.6).

Inlet pressure and temperature distortion limits were not exceeded during ground run or during hover, helicopter, and conversion mode flight. Temperature distortion limits were not exceeded in airplane mode, and were not exceeded during any test point during Phase I. Since inlet temperature distortion levels remained nearly constant during all test points, it was concluded that inlet temperature distortion and inlet temperature rise effects on inlet performance were negligible. During airplane mode flight, there were several test points where the inlet pressure distortion levels exceeded the allowable limit and are evident in Figure 3.6. These test points in question were with the bypass door open, and it was observed that pressure distortion levels increased as airspeed increased when the bypass door was open. Pressure distortion levels were acceptable in all other flight modes and conditions.

To alleviate concerns of inlet pressure distortion during Phase II testing, a limitation on the corrected gas-generator speed of the engine compressor was imposed when the aircraft was in airplane mode cruise with the bypass door open. Corrected gas-generator speed was found by dividing the gas generator speed Ng by the square root of the temperature ratio θ (Equation 3.6):

$$Ng_C = \frac{Ng}{\sqrt{\theta}} \tag{3.6}$$

A design change of the inlet plenum to further lower the inlet pressure distortion levels during high airspeed airplane-mode cruise and remove the corrected gas-generator speed limit was tested during Phase III, and will be discussed in more detail in Section 3.3.1.

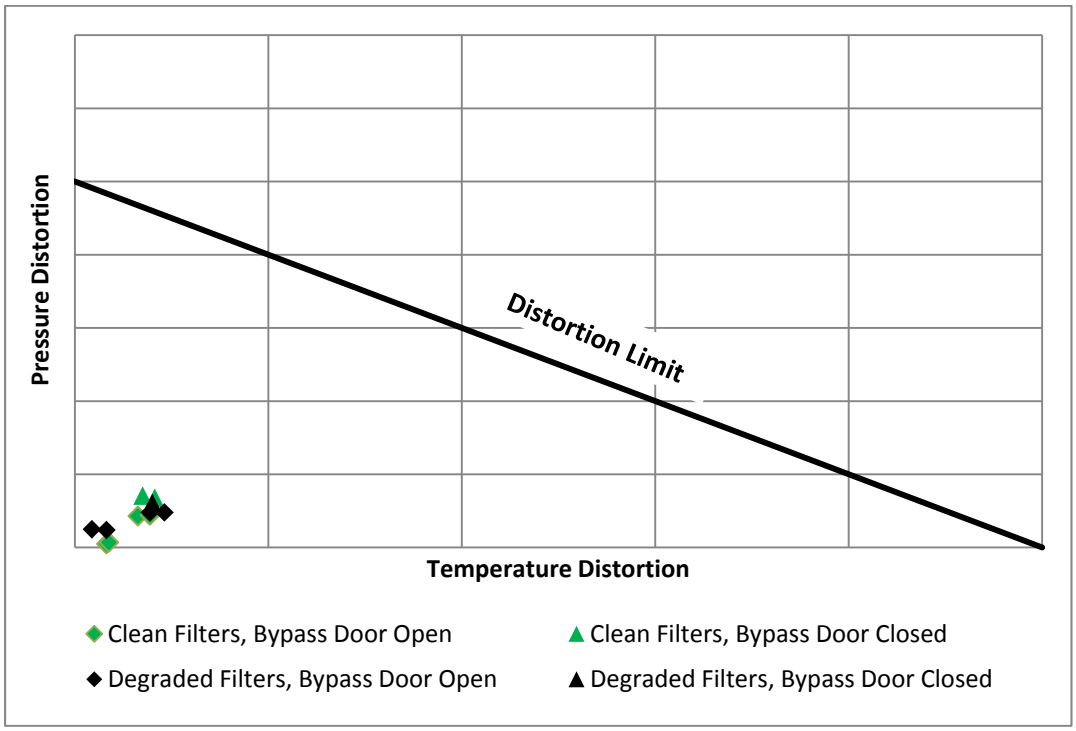

Figure 3.4 Phase I Ground Run Inlet Distortion

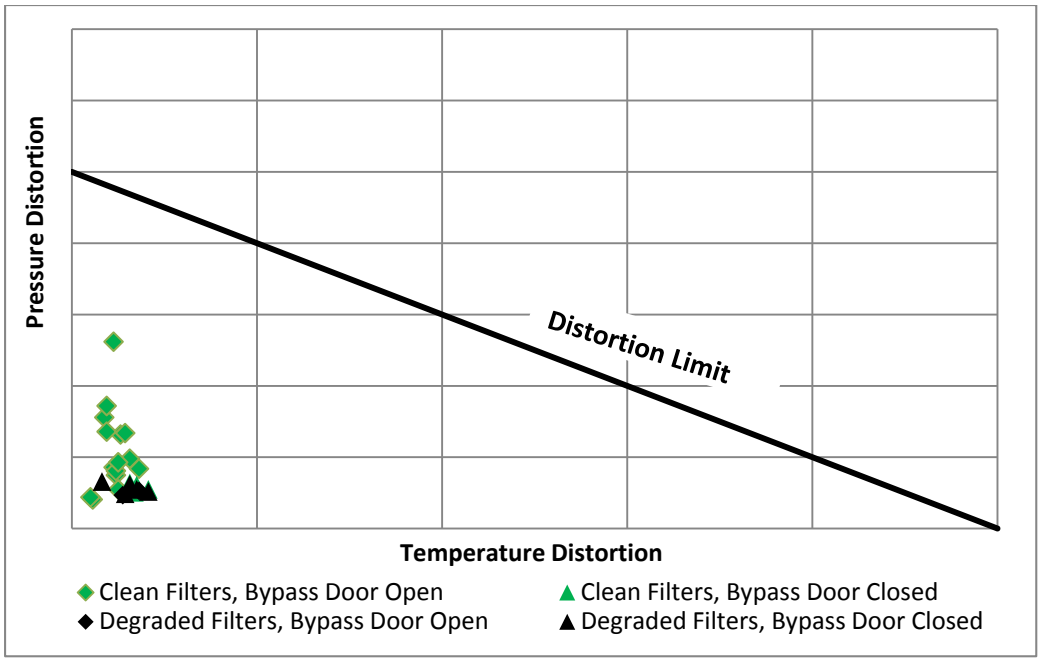

Figure 3.5 Phase I Hover, Helicopter, and Conversion Mode Inlet Distortion

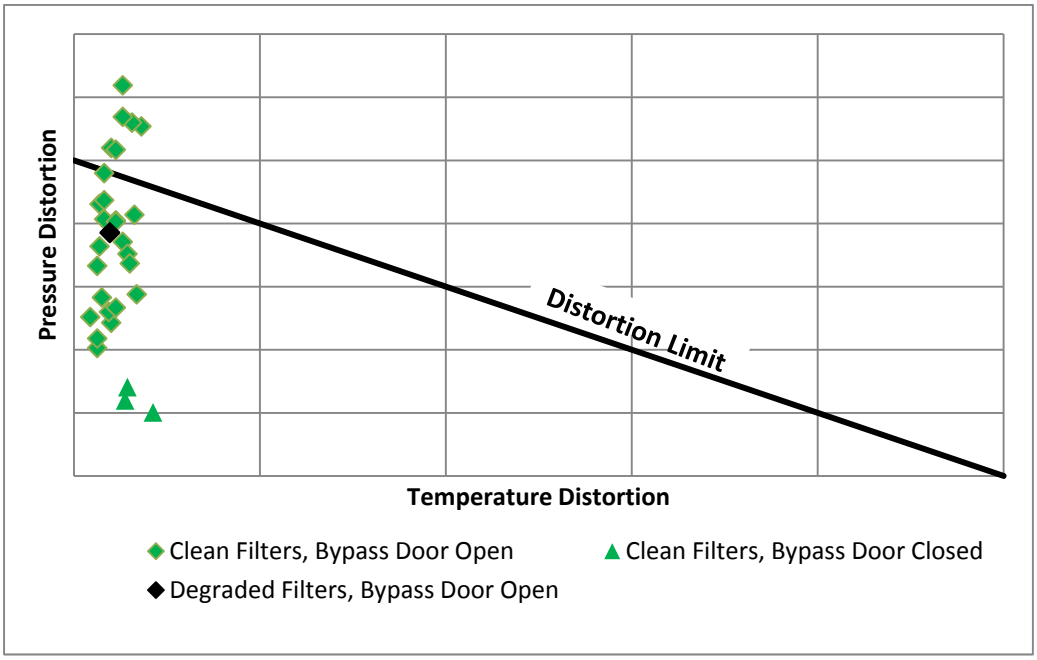

Figure 3.6 Phase I Airplane Mode Inlet Distortion

3.1.4 Inlet Pressure Recovery

3.1.4.1 Data Reduction

Inlet pressure recovery was calculated by the author using CAFTA, which was found by dividing the total pressure measured at the inlet face by the free stream total pressure during prime records of steady state maneuvers. Total pressure measured at the inlet face was computed by taking the average of the 40 engine inlet rake total pressures during each steady state prime record. Scatter in the inlet recovery data was minimal, but the small scatter can likely be attributed to differences in engine power required for each test point, as well as differences in OAT and Hp over each test day.

3.1.4.2 Results and Discussion

Calculated inlet pressure recovery values were plotted by the author as a function of inlet pressure recovery and airspeed; this plot is shown in Figure 3.7. The scatter in inlet pressure recovery measured during hover was within 0.5% for clean filters and within 1% with simulated degraded filters. In airplane mode cruise, inlet pressure recovery decreased as airspeed increased, with the degraded filters having comparable performance to clean filters.

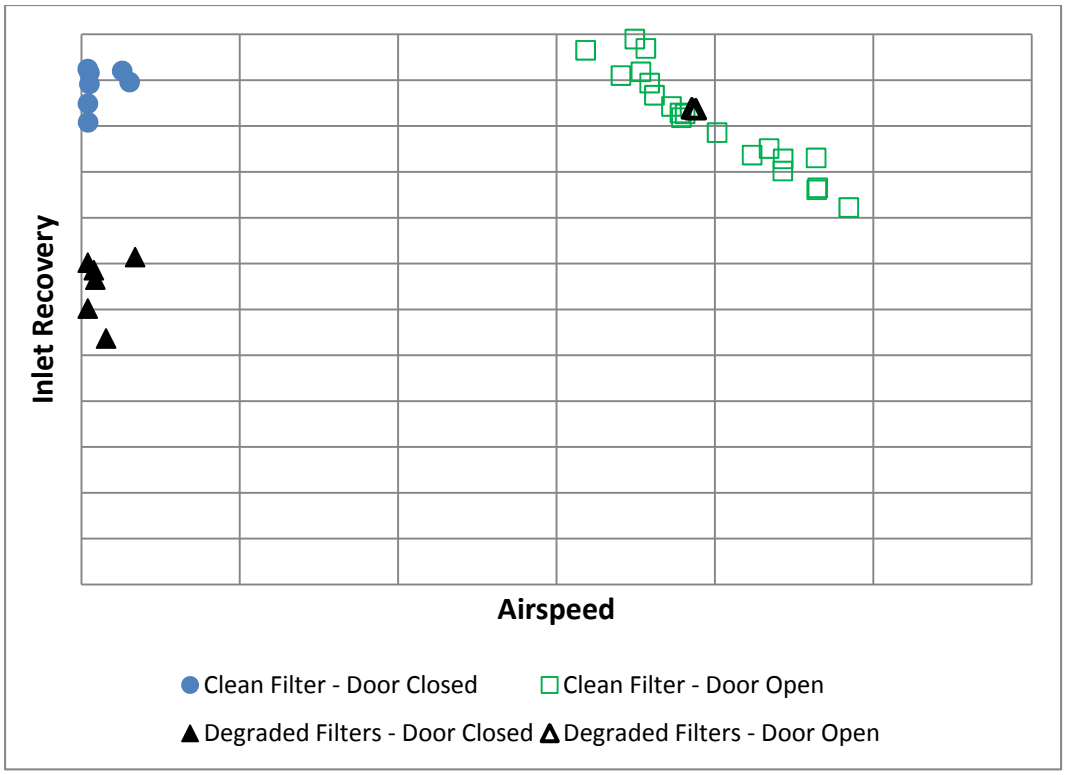

Figure 3.7 Inlet Pressure Recovery for Phase I EIBF Configuration

3.1.5 Power Assurance Check

3.1.5.1 Data Reduction

Engine power available performance was calculated and recorded upon command by the pilot using a Bell proprietary Power Assurance Check (PAC) algorithm that is programmed in VSLED. PAC points can be taken in either a hover or in airplane mode cruise and are considered equivalent to each other (i.e. a hover PAC number can be directly compared to a cruise PAC number). VSLED automatically detects the flight mode and outputs engine power available as a percentage of engine torque to a specified reference value, with higher percentage indicating better engine performance. The variables that drive PAC values for aircraft in general are Measured Gas Temperature (MGT), along with OAT and Hp.

The PAC calculated by VSLED has a known scatter range, which is shown by the scatter bars in Figures 3.9 and 3.10. This scatter can be attributed to one or a combination of several factors: differences in thermal stability period, as well as variations in Hp and OAT. For an optimal PAC, it is desired for the engine to achieve steady-state thermal stability. Due to constraints on resources and the fact that this was only a proof-of-concept test rather than a detailed qualification, the stabilization period was limited at times, which could be a contributor to PAC scatter. Additionally, the scatter will be less if the PAC was repeated at the exact Hp and OAT conditions. These environmental variables obviously varied from each flight test day, which led to some inherent scatter in the test data.

3.1.5.2 Results and Discussion

PAC data collected from Phase I VSLED data is displayed in Figure 3.8, with PAC plotted against Phase I flight number. Power Assurance Check numbers during flight #0 were measured in the test cell of the engine manufacturer, when the engines were shipped outbound for installation on the aircraft, with flight numbers increasing in sequential order as they are flown during Phase I. The degraded inlet filters were installed on the #1 engine during flight #6, and all PAC measurements were taken with the bypass door closed. Since Phase I placed a heavier emphasis on collecting inlet performance data over PAC data, PAC points were typically only collected at the beginning and end of each flight.

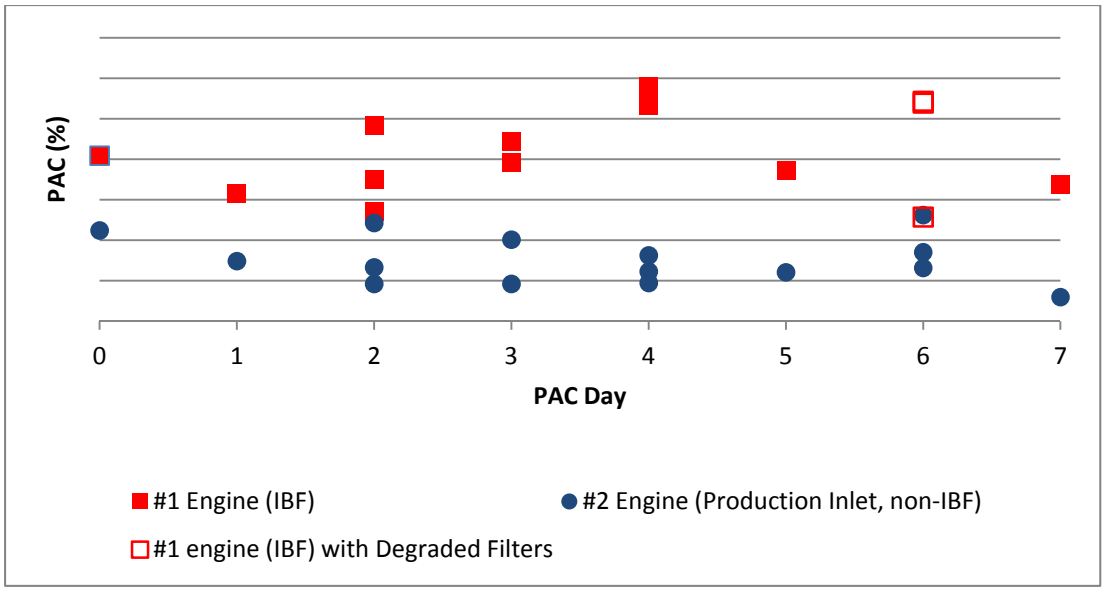

Figure 3.8 Phase I PAC Data

The PAC data displayed in Figure 3.8 was separated for the #1 and #2 engines in Figures 3.9 and 3.10, with error bars were drawn on the outbound test cell data to represent the scatter range. The data collected during the flight tests fit within the scatter range of the outbound test cell data for both engines. Only one PAC from the #2 engine during test #7 was slightly outside of the scatter bar. Since all the PAC points taken during flight test fell within (or reasonably within) the scatter of the outbound test cell data, it can be concluded with reasonable certainty that the prototype EIBF system does not have an adverse impact on engine power available performance.

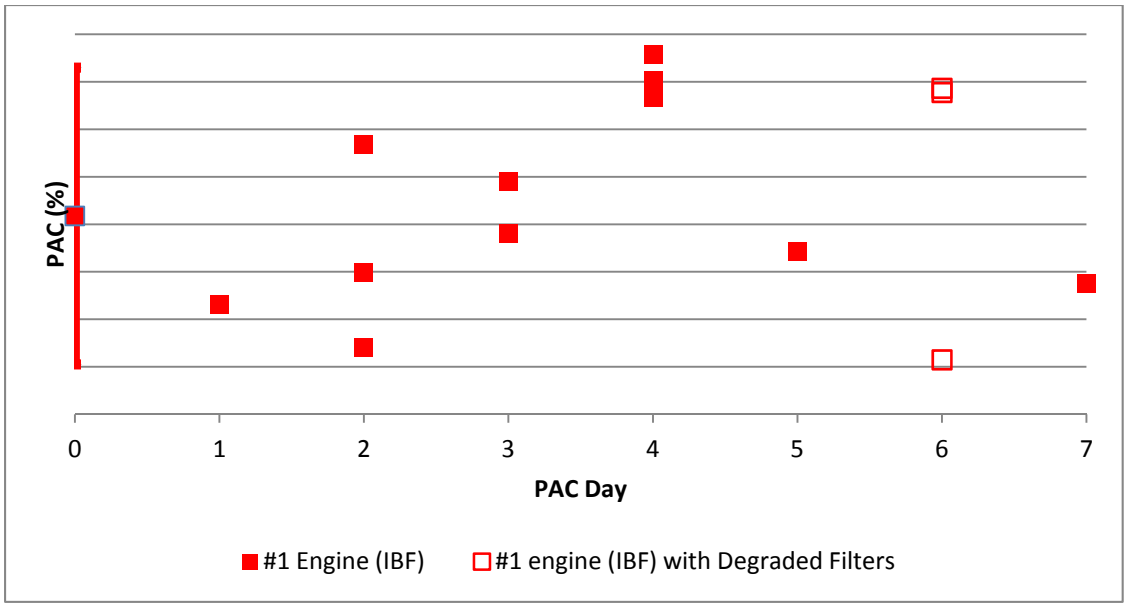

Figure 3.9 Phase I #1 engine PAC

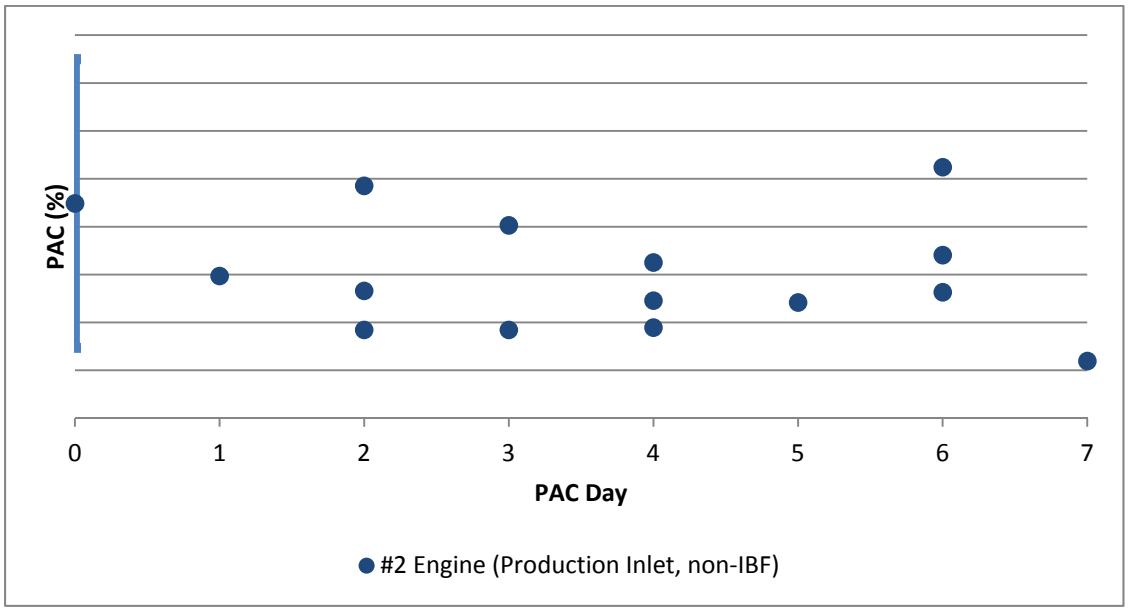

Figure 3.10 Phase I #2 engine PAC

3.2 Phase II

3.2.1 Purpose of Test and Test Conditions

Phase II was conducted at Kirtland Air Force Base (KAFB) in Albuquerque, NM. This phase of testing focused on evaluating the performance of the filters installed on the #1 engine, and comparing engine power deterioration to the #2 engine with the current production EAPS installed. Historically, helicopter engines have seen heightened rates of compressor blade corrosion and engine deterioration at KAFB due to the fine sand and particulate matter found in the Albuquerque area, leading to its selection as the site for this phase of the flight test program. For Phase II, a pre-determined flight profile was flown over the austere sand environment and repeated until the bypass door was automatically commanded open due to the filters getting clogged by the sand after prolonged exposure in the austere environment. This marked the completion of one filter cycle, and the procedure was repeated for several filter cycles. A clean set of filters was installed on the #1 engine prior to commencing Phase II flight testing, and was replaced at the end of each filter cycle. The inlet rake was removed for this phase of flight testing to reduce risk of foreign object damage (FOD); demonstrating engine stability in Phase I so that the inlet rake could be removed for Phase II was a prerequisite.

The Phase II flight profile was developed in conjunction with KAFB pilots and is depicted in Figure 3.11. The flight profile was designed to accelerate engine deterioration in an austere environment, and consisted of the following maneuvers:

1) Steady Hover at 50 feet
2) Steady Hover at 20 feet
3) Land in austere environment with rotors turning

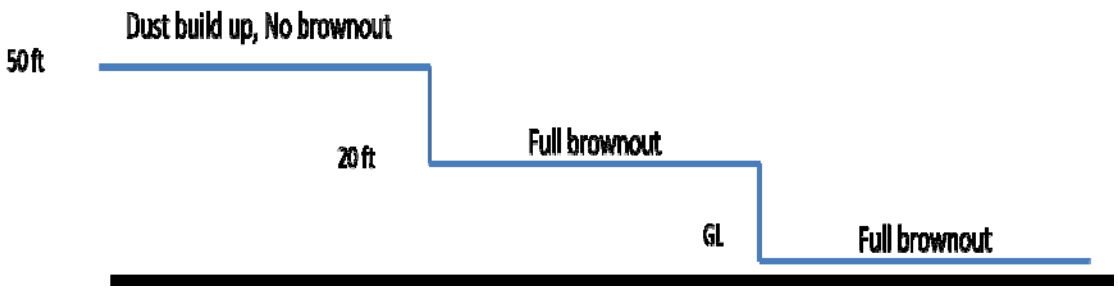

Figure 3.11 Flight Profile in Austere Environment (Phase II)

3.2.2 Flight Test Results

The test team successfully completed numerous filter cycles in the austere environment without any instances of abnormal operation on the #1 engine (Figure 3.12). Figure 3.13 shows pictures of the filters prior to the start of testing in the austere environment as well as the same filters at the end of a filter cycle.

Figure 3.12 ATTR Landing in Austere Environment

Figure 3.13 Filters before and after bypass trip (blanking plates on opposite side)

3.2.3 Power Assurance Check

3.2.3.1 Data Reduction

The same data reduction technique described in section 3.1.5.1 was used.

3.2.3.2 Results and Discussion

PAC data collected from Phase II is shown in Figure 3.14 as a function of PAC versus time in austere environment. From this figure, it can be visibly noticed that the #1 engine sustained less deterioration in PAC when compared to the #2 engine. The noticeable consistency in engine health of the engine with the prototype EIBF system installed demonstrates that when compared to the current production inlet, the prototype EIBF system is more effective in maintaining engine power in an austere environment. Given this, the benefits of the prototype EIBF is starting to be realized.

It is also projected that the prototype EIBF system will require less maintenance manhours compared to the current production inlet. The #2 engine required 2.8 times more manhours of maintenance when compared to the #1 engine. The engine PAC data collected during Phase II testing demonstrates that the prototype EIBF system extends engine TOW, with the additional benefit of reducing maintenance man hours and depot maintenance time.

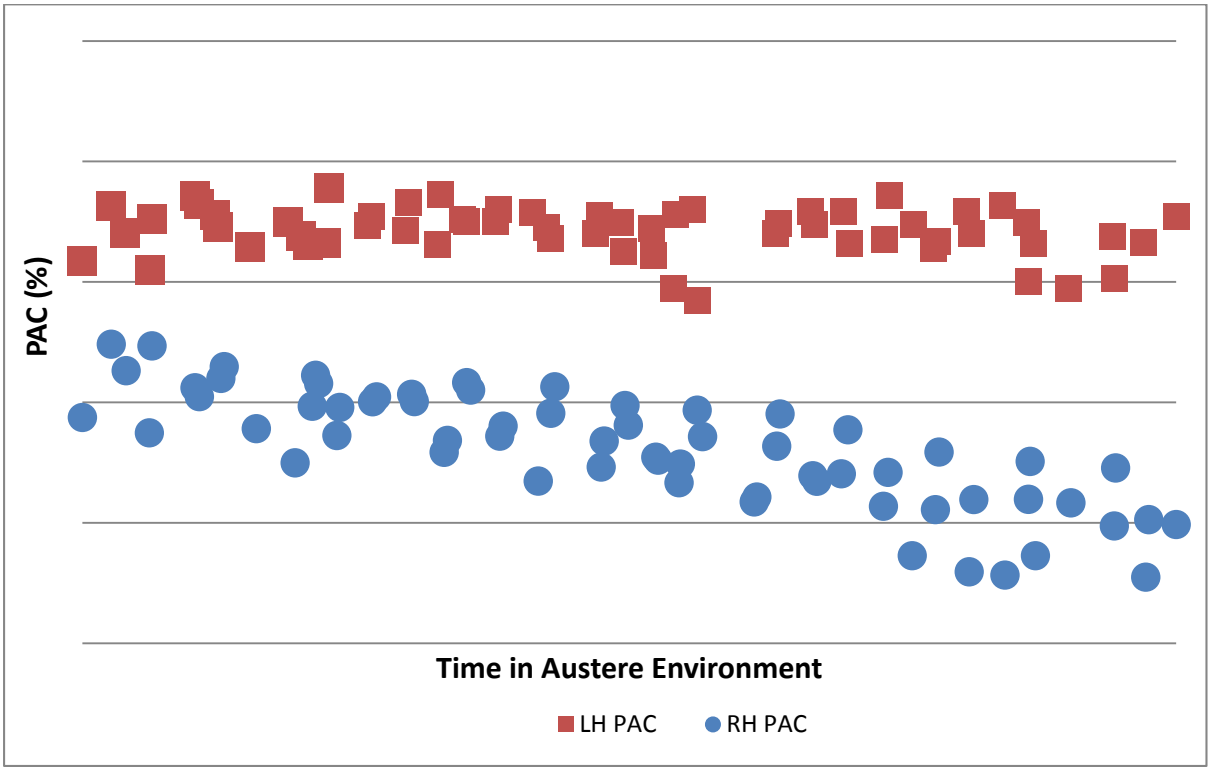

Figure 3.14 Phase II PAC Data

3.3 Phase III

3.3.1 Purpose of Test and Test Conditions

While Phase I demonstrated the feasibility of the prototype EIBF installation, elevated inlet pressure distortion levels during test points in airplane mode cruise with the bypass door open remained a challenge. From the data collected from the inlet rake and reduced by the author during Phase I and additional CFD simulations that were conducted, it was determined that it was necessary to direct more airflow to the upper portion of the inlet plenum to lower the inlet pressure distortion levels during airplane mode cruise with the bypass door open. Several design solutions were conceived and tested in CFD models, and it was found that inlet guide vanes installed in the inlet plenum were the best solution to direct additional airflow to the low pressure region and further lower the inlet pressure distortion levels. Prior to starting Phase III flight tests, inlet guide vanes were installed; the blanking plates and inlet duct extensions described in sections 3.1.2.1 and 3.1.2.2 were left installed on the aircraft. The inlet rake assembly was reinstalled in the bellmouth of the #1 engine, and a smaller matrix of test points was flown. These test points consisted primarily of airplane mode cruise with the bypass door open. The objective of this flight testing phase was to ensure that the inlet pressure distortion levels during airplane mode cruise with the bypass door open fell below acceptable limits so that the corrected gas-generator speed restriction described in section 3.1.3.2 could be removed.

3.3.2 Flight Test Results

The inlet guide vanes alleviated the inlet pressure distortion to acceptable levels in airplane mode cruise with the bypass door open while maintaining stable engine operation, which allowed the corrected gas-generator speed restriction to be removed. The following sections discuss inlet distortion improvements, as well as inlet pressure

recovery. Inlet temperature distortion and Power Assurance Checks are not discussed in this section, since adequate inlet temperature distortion margin and engine power were maintained during Phase I flight testing.

3.3.3 Inlet Pressure Distortion

3.3.3.1 Data Reduction

The same data reduction technique described in section 3.1.3.1 was used.

3.3.3.2 Results and Discussion

Inlet pressure distortion ratio is defined as the measured pressure distortion divided by the engine specification limit. Since all test points collected in Phase III were in airplane mode with the bypass door open, Phase III pressure distortion data will be plotted as a function of airspeed by the author; data from similar test points in Phase I was reduced by the author using the same methodology for comparison to the data collected in Phase III. Figure 3.15 shows the inlet pressure distortion ratio plotted as a function of airspeed for all Phase I and III test points in airplane mode cruise with the bypass door open, with the black line indicating the distortion limit set forth by the engine specification. The inlet pressure distortion ratio increases as airspeed increases; inlet pressure distortion ratios computed from flight test was compared to CFD simulations at similar flight conditions and airspeeds and was found to correlate closely. The inlet guide vanes were sufficient to remove the corrected gas-generator speed restriction on the aircraft, and the data reduction that was completed by the author gave the test team confidence that analytical tools such as CFD can be used to further refine the prototype EIBF system into a final production design that will have lower pressure distortion levels than what was measured during this testing.

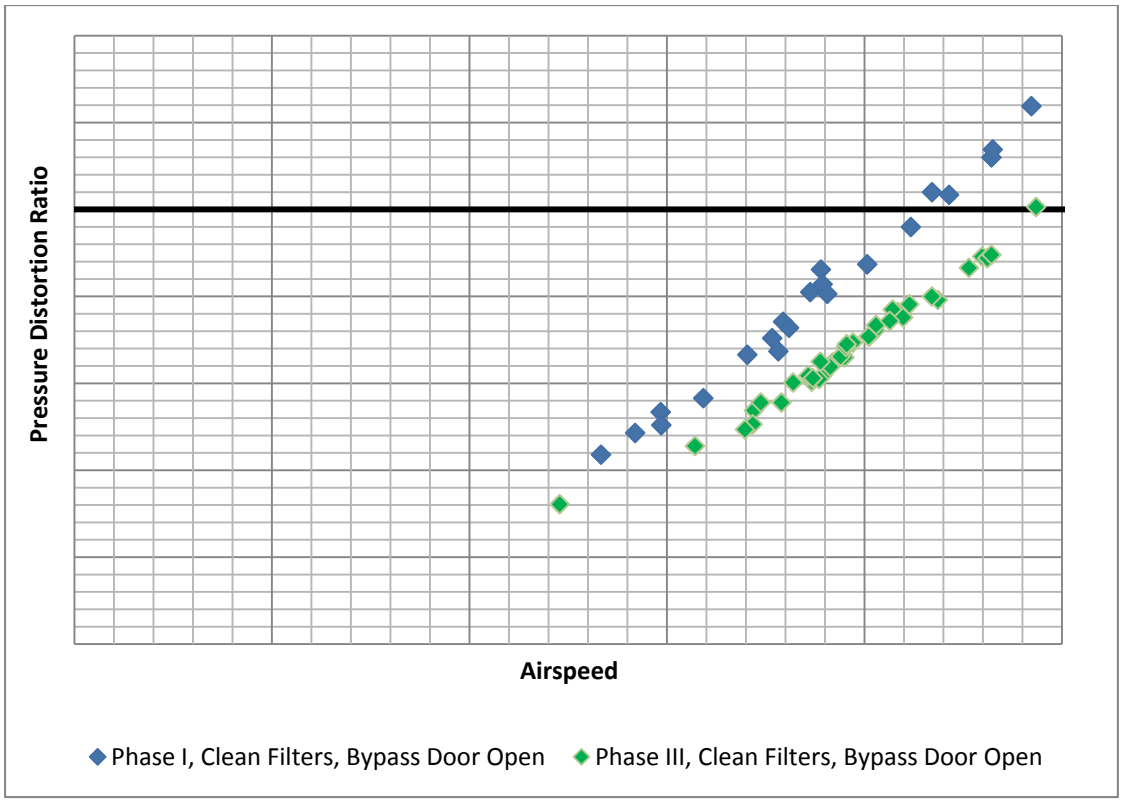

Figure 3.15 Comparison of Phase I and Phase III Inlet Distortion in Airplane Mode, Bypass Door Open

3.3.4 Inlet Pressure Recovery

3.3.4.1 Data Reduction

The same data reduction technique described in section 3.1.4.1 was used.

3.3.4.2 Results and Discussion

Inlet pressure recovery measured during Phase III was plotted in the same manner by the author as the Phase I inlet pressure recovery reported in section 3.1.4.2, and is shown in Figure 3.16 with the Phase I data overlaid for reference. Overall, the inlet pressure recovery between the two configurations is comparable at lower airspeeds, with the inlet recovery measured at higher airspeeds during Phase III to be slightly lower than what was measured during Phase I. Data collected during Phase III followed the same

trend of that in Phase I in that inlet recovery decreased as airspeed increased. The vane installed during Phase III allowed the corrected gas-generator speed restriction to be removed while still providing adequate power levels, demonstrating that an inlet barrier filter installation for a tiltrotor application is feasible. As discussed in section 1.3, inlets are designed to maximize pressure recovery, so to minimize impact on engine power available, lessons learned will be incorporated into a final production EIBF design that will have adequate inlet distortion margin along with improved inlet pressure recovery than what was measured in Phase III.

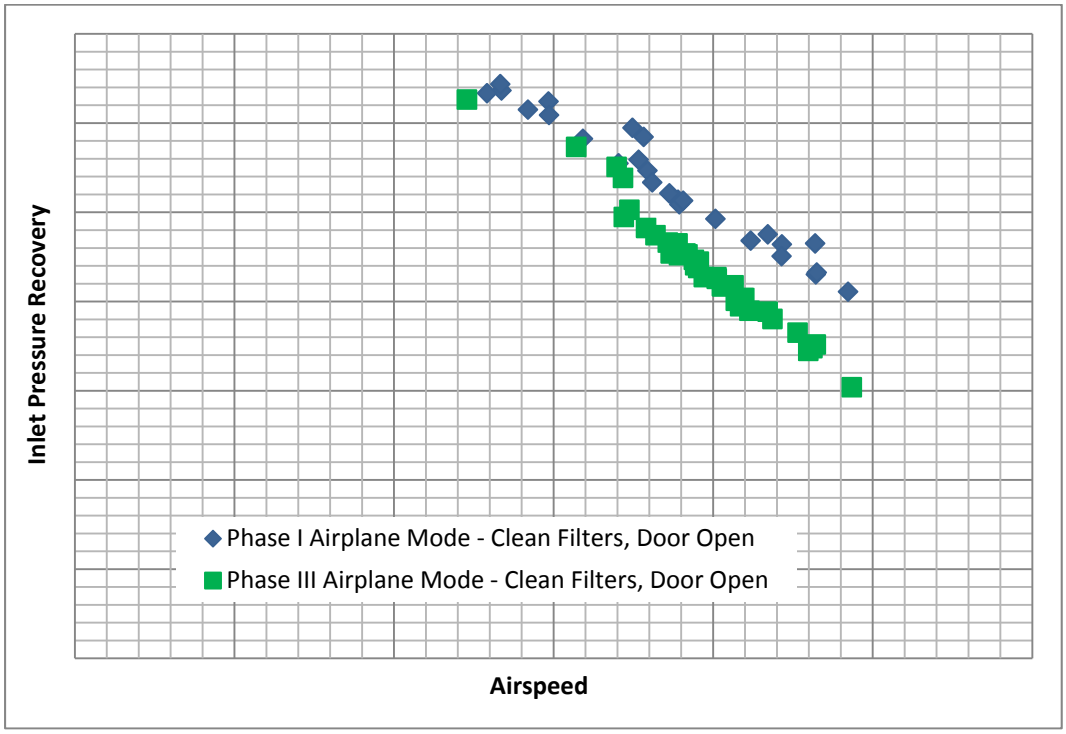

Figure 3.16 Comparison of Phase I and III Inlet Pressure Recovery in Airplane Mode, Bypass Door Open

3.4 Phase IV

3.4.1 Purpose of Test and Test Conditions

Phase IV was conducted at Eglin Air Force Base near Pensacola, FL. This phase of flight testing was focused on evaluating the performance of the filters installed on the #1 engine, and comparing engine power deterioration to the current production EAPS on the #2 engine in a saltwater environment, in a similar fashion to what was conducted in Phase II. Donaldson filters have a history of improving engine performance on offshore race boats; they incorporated similar features into the filters manufactured for these flight tests. Donaldson conducted laboratory tests to show that this technology would yield similar results for aerospace applications, thus given the fact that salt particle build-up causes engine deterioration just like sand particles, it was of interest to demonstrate the performance of the prototype EIBF installation in a saltwater environment.

Two flight profiles were created for Phase IV flight testing: the safety of flight profile (Figure 3.17) and the notional Phase IV flight profile (Figure 3.18). The inlet rake was removed prior to commencing the flight test, due to FOD concerns. The time-in-environment profile was conducted first, starting at 100 feet above the seawater and descending to lower altitudes in 10 foot increments in a conservative buildup fashion until 50 feet above the seawater. Based on favorable outcomes from the time-in-environment profile, the notional Phase IV flight profile would then be conducted in a similar fashion to the time-in-environment profile. The lowest permissible distance above the saltwater will be 10 feet; however the actual lowest permissible altitude will be determined during flight test based on the weather and sea-state conditions.

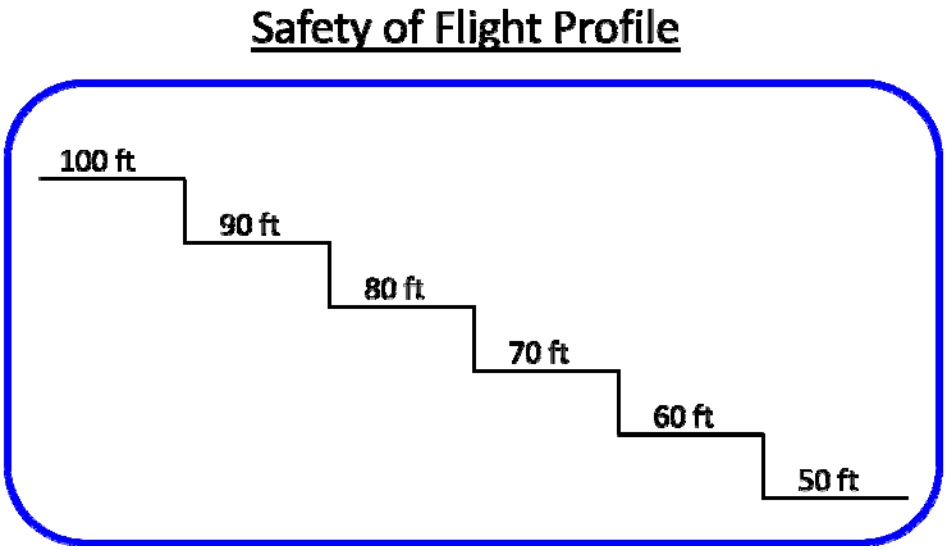

Figure 3.17 Safety of Flight Profile

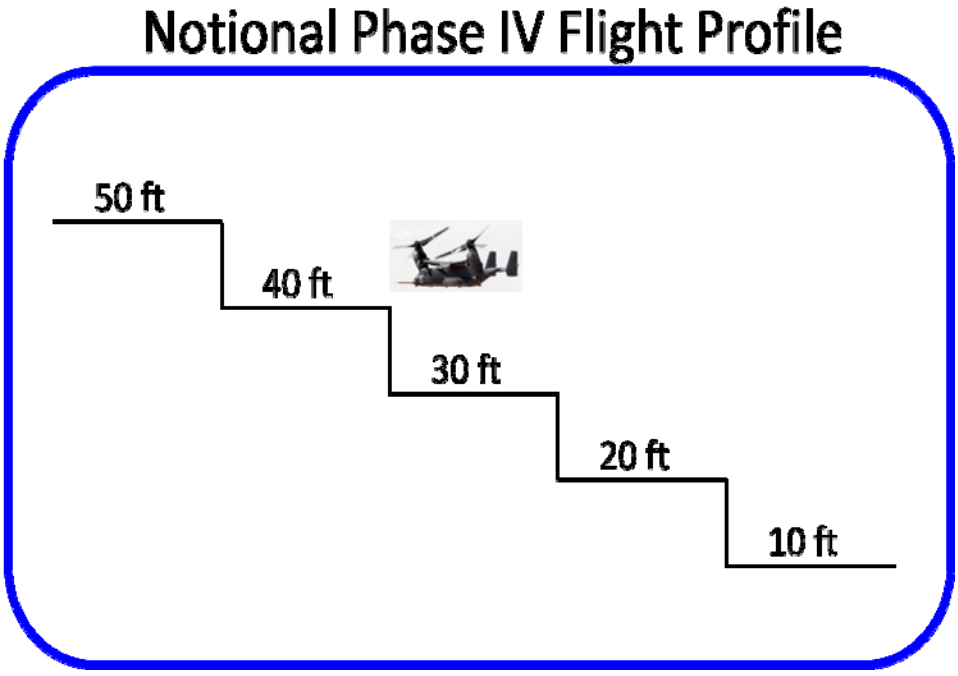

Figure 3.18 Notional Phase IV Flight Profile

3.4.2 Flight Test Results

Figure 3.19 shows a picture of the test aircraft hovering in the saltwater environment. During the safety-of-flight profile, the pilots reported that salt spray was not as severe as expected at this altitude and a negligible impact on power reduction in both engines was observed. The Phase IV flight profile was completed during the second and third flights; the environmental conditions allowed the aircraft to descend between 30 and 40 feet above the seawater (Figure 3.20). The results presented in the next section will exclusively focus on the data collected from the two flights where the flight profile depicted in Figure 3.20 was conducted.

Figure 3.19 ATTR hovering over Saltwater Environment

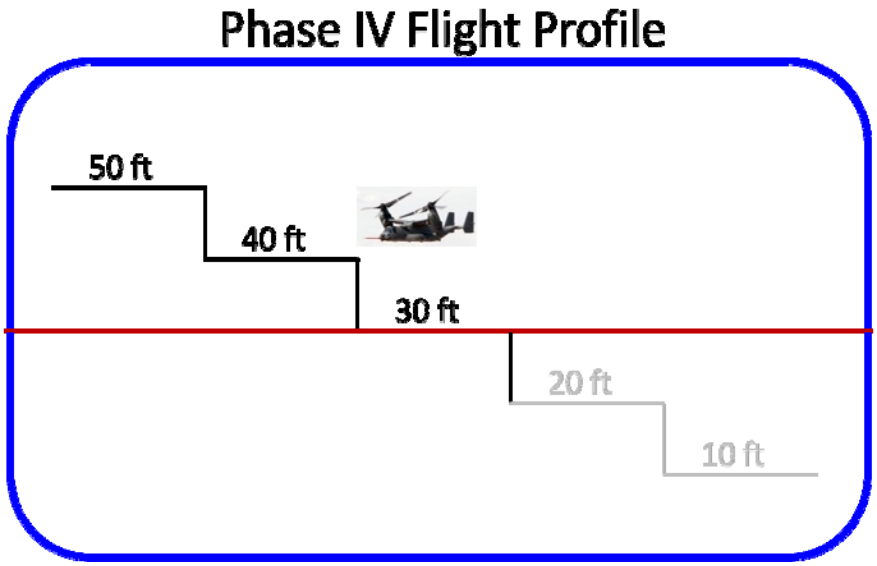

Figure 3.20 Phase IV Flight Profile

3.4.3 Power Assurance Check

3.4.3.1 Data Reduction

The same data reduction technique described in section 3.1.5.1 was used.

3.4.3.2 Results and Discussion

PAC data collected from two flights where the Phase IV profile was flown is shown in Figure 3.21 as a function of PAC vs. time in saltwater environment with the black line separating between the second and third flight test. The trend observed during saltwater environment testing (Phase IV) is similar to what was observed during austere environment testing (Phase II) in that the #1 engine maintains a steady PAC more easily than the #2 engine. This shows that the filters are effectively able to capture salt particulates in addition to sand particulates, and that this testing demonstrates that the prototype EIBF installation is more effective than the current production EAPS inlet in maintaining engine power in a saltwater environment.

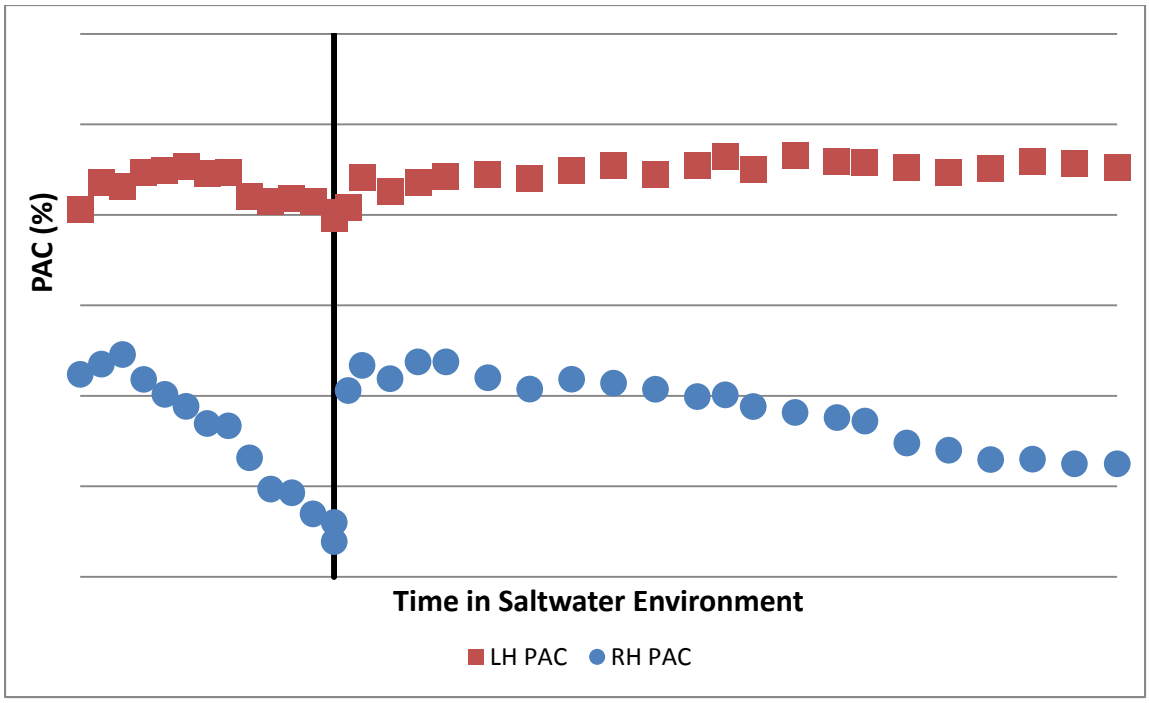

Figure 3.21 Phase IV PAC Data

Chapter 4

CONCLUSIONS AND FUTURE WORK

Flight testing of the prototype EIBF installation was completed through four phases of flight testing, which successfully demonstrated the objectives stated in Section 2.1 and are summarized below.

Objective 1: Ensure safety of flight with the prototype EIBF installation, including aircraft, engine, and EIBF bypass door operation

a) Safety of flight of the entire aircraft was ensured throughout all 4 phases of flight testing, with both engines operating as expected.

b) The bypass door operated as expected. No adverse engine events or surges occurred at any time during the flight testing, and the bypass door opened during airplane mode cruise. Phase II flight testing demonstrated that the bypass door functioned as intended in an austere environment when the filters became clogged with sand.

Objective 2: Ensure adequate inlet and engine performance, including pressure recovery, inlet pressure distortion, and engine power levels.

a) Inlet pressure recovery computed by the author on the #1 inlet was adequate and comparable to data collected in previous testing on the current production EAPS.

b) Inlet pressure and temperature distortion computed by the author were below the limits prescribed by the engine manufacturer for the #1 engine. Based on Phase I data collected, the inlet design was further refined and tested during Phase III to improve inlet pressure distortion during airplane mode with the bypass door open.

c) Adequate engine power levels were maintained on both engines during all 4 phases of flight testing.

Objective 3: Compare degradation of the engine with the prototype EIBF installed to the engine without the inlet barrier filter installed.

a) Engine PAC data collected during Phase I demonstrated that the #1 and #2 engine power levels were comparable in a clean-air environment. Engine PAC data collected during Phases II and IV showed that the #2 engine deteriorated quicker than the #1 engine in the austere and saltwater environments, thus validating the effectiveness of the prototype EIBF installation in increasing engine time-on-wing.

This proof-of-concept flight testing successfully satisfied all flight test objectives and demonstrates the feasibility of the prototype EIBF installation, which led to a contract award by the US Navy for the Bell Boeing team to develop a final inlet barrier filter configuration. The data collected during flight test correlated well with data collected from CFD, and demonstrates that analytical tools along with lessons learned from the proof-of-concept flight testing (blanking plates, bypass duct extensions, and inlet guide vanes) can be used to make further refinement and optimize a final inlet barrier filter configuration. Inlet air filtration with an inlet barrier filter is expected to quadruple TOW by preventing nearly all fine particulates from entering the engine, which will yield an increase in tiltrotor operational capability and readiness, while decreasing tiltrotor maintenance downtime and consequently decreasing costs.

Appendix A

INLET RAKE GEOMETRY

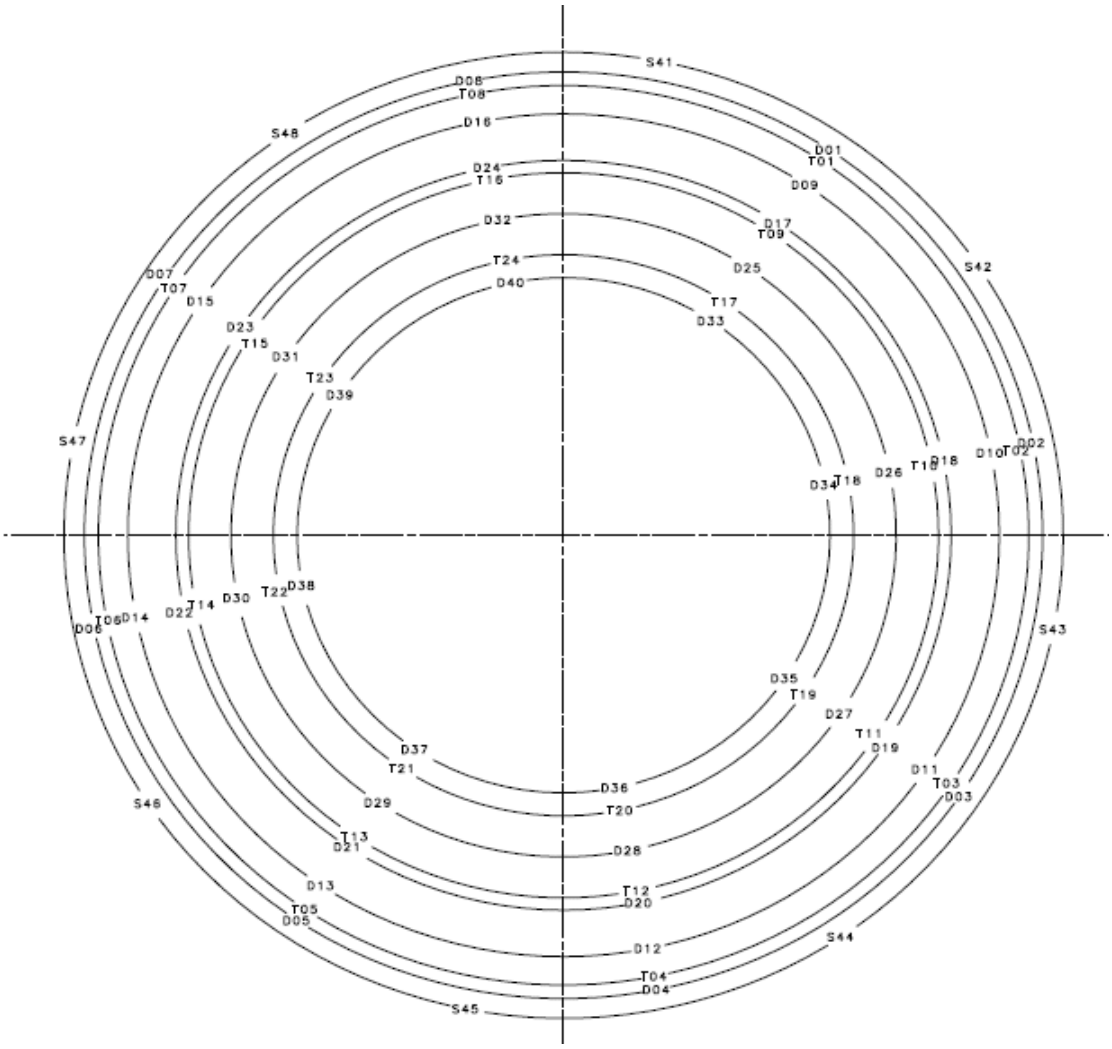

Figure A.1 Schematic showing Locations of Pressure and Temperature Probes

(Forward Looking Aft View)

Table A.1 Inlet Rake Total Temperature Probes

No.	Reference No.	Angle
1.	D01	33.75
2.	D02	78.75
3.	D03	123.75
4.	D04	168.75
5.	D05	213.75
6.	D06	258.75
7.	D07	303.75
8.	D08	348.75
9.	D09	33.75
10.	D10	78.75
11.	D11	123.75
12.	D12	168.75
13.	D13	213.75
14.	D14	258.75
15.	D15	303.75
16.	D16	348.75
17.	D17	33.75
18.	D18	78.75
19.	D19	123.75
20.	D20	168.75
21.	D21	213.75
22.	D22	258.75
23.	D23	303.75
24.	D24	348.75
25.	D25	33.75
26.	D26	78.75
27.	D27	123.75
28.	D28	168.75
29.	D29	213.75
30.	D30	258.75
31.	D31	303.75
32.	D32	348.75
33.	D33	33.75
34.	D34	78.75
35.	D35	123.75
36.	D36	168.75
37.	D37	213.75
38.	D38	258.75
39.	D39	303.75
40.	D40	348.75

Table A.2 Inlet Static Pressure Probes

No.	Reference No.	Angle
1.	S41	11.25
2.	S42	56.25
3.	S43	101.25
4.	S44	146.25
5.	S45	191.25
6.	S46	236.25
7.	S47	281.25
8.	S48	326.25

Table A.3 Inlet Total Temperature Probes

No.	Reference No.	Angle
1.	T01	33.75
2.	T02	78.75
3.	T03	123.75
4.	T04	168.75
5.	T05	213.75
6.	T06	258.75
7.	T07	303.75
8.	T08	348.75
9.	T09	33.75
10.	T10	78.75
11.	T11	123.75
12.	T12	168.75
13.	T13	213.75
14.	T14	258.75
15.	T15	303.75
16.	T16	348.75
17.	T17	33.75
18.	T18	78.75
19.	T19	123.75
20.	T20	168.75
21.	T21	213.75
22.	T22	258.75
23.	T23	303.75
24.	T24	348.75

References

1) *V-22 Osprey Guidebook, 2013/2014.* Available from http://www.bellhelicopter.com/MungoBlobs/126/268/V-22%20Guidebook%202013_update_PREVIEW_LR2.pdf. Internet; accessed 29 September 2014.

2) "V-22 Osprey – 070427-N-0841E-011". *Boeing: Image Gallery*. Available from http://www.boeing.com/boeing/companyoffices/gallery/images/military/rotorcraft/v22/070427-N-0841E-011.page?. Internet; accessed 29 September 2014.

3) "AE 1107". *Rolls-Royce*. Available from http://www.rolls-royce.com/defence/products/helicopters/ae_1107/. Internet; accessed 29 September 2014.

4) "V-22 Osprey". *Boeing: Image Gallery*. Available from http://www.boeing.com/boeing/companyoffices/gallery/images/military/rotorcraft/v22/navairCV-22_aerial_41.page?. Internet; accessed 29 September 2014.

5) Mattingly, Jack D. *Elements of Propulsion: Gas Turbines and Rockets.* AIAA Education Press, 2006.

6) SAE International. *Gas Turbine Engine Inlet Flow Distortion Guidelines, Rev. B*. 2002.

7) Augustin, M. and Phillips, J. "The V-22 Vibration, Structural Life, and Engine Diagnostic System, VSLED." SAE Technical Paper 871732, 1987.

Biographical Information

Victor Hwa grew up in East Brunswick, NJ. After graduating from East Brunswick High School in 2005, Victor attended The University of Texas at Austin, where he graduated with a Bachelor of Science in Aerospace Engineering and a Minor in Business in May 2010. In June 2010, Victor started working for Bell Helicopter Textron in the Propulsion Structures Design group, and started to pursue a Master of Science Degree in Aerospace Engineering at The University of Texas at Arlington in January 2011, while concurrently being employed with Bell. In March 2011, Victor moved to the Propulsion Analysis and Engine Integration group, where his work has focused on Engine Performance Analysis and Trade Studies, Computational Fluid Dynamics, and Flight Testing over a wide range of engine platforms on a variety of aircraft. Currently, Victor is an Aircraft Systems Engineer for the V-22 program and has previously worked the H-1 Upgrade program.

In his spare time outside of work, Victor enjoys snowboarding, running, and cycling. He also enjoys travelling, both domestically and internationally.